Nuclear Magnetic Resonance Characterization of the Myristoylated, N-Terminal Fragment of ADP-Ribosylation Factor 1 in a Magnetically Oriented Membrane Array†

Judit A. Losonczi and James H. Prestegard*

Department of Chemistry, Yale University, New Haven, Connecticut 06520

Received July 22, 1997; Revised Manuscript Received October 31, 1997⊗

ABSTRACT: The behavior of the N-terminal fragment of human ADP-ribosylation factor 1 (ARF1) in a membranelike environment is described. This is accomplished using heteronuclear liquid crystal NMR techniques in a magnetically oriented membrane array on a selectively ^{13}C- and ^{15}N-labeled peptide. After full assignment of the labeled sites, residual dipolar couplings ($^{13}C-^{13}C$, $^{15}N-^{1}H$ and, $^{13}C-^{15}N$) and chemical shift anisotropy effects (amide ^{13}C and ^{15}N) were measured. The experimental data were interpreted using order matrix calculations to yield orientational and dynamic information for four separate, rigid amide planes. The experimental data obtained proves that the amphipathic peptide interacts with the bilayer in a mode that is consistent with an α-helix having its axis parallel to the membrane surface. Possibilities of extending the employed techniques to larger and uniformly labeled systems are discussed.

A large number of proteins in living cells are membrane-associated; they can be loosely associated peripheral proteins, they can be surface proteins with one or more lipid derived anchors, or they can be integral proteins with substantial transmembrane segments. All play important and highly diverse roles in cellular processes such as transport of metabolites, ion pump mechanisms, and regulation of the intracellular environment (*1*). Here we focus on a fragment from human ADP-ribosylation factor 1 (ARF1), a surface protein that is anchored to the membrane by an N-terminal myristoyl chain. We attempt to provide a structural description using relatively new NMR methods applicable in a membranelike environment.

To understand the detailed function and biological properties of membrane proteins like ARF1, it is important to have high-resolution structural information. Because many of these proteins are only soluble, or biologically viable, in a membranelike environment, they must be studied in systems with at least the minimal characteristics of the lipid bilayers on which most membranes are based. A number of methods are available to study these proteins (*2*), including electron microscopy, for which the achieved resolution is low (*3*), and X-ray diffraction, for which difficulties in crystallizing membrane-bound proteins often arise (*4*).

NMR methodology approaches the problem of studying membrane proteins from two directions. One is to use detergent micelles to mimic a membranelike environment. Peptides and proteins in these systems reorient fast enough to give sufficient resolution for multidimensional solution NMR experiments and traditional nuclear Overhauser effect-(NOE-) based structural determinations can be pursued (*5*). Because of the small diameter of the micelles, however, questions arise about their relationship to the nearly planar surface of biological membranes. The other approach employs solid-state NMR methods on oriented and unoriented samples of proteins in hydrated phospholipid bilayers to acquire either distance or angular constraints via the measurements of dipolar couplings and chemical shift anisotropy effects (*6*−*8*). From these experiments it is possible to get data on the relative arrangement of major secondary structure elements or the relative orientation of a major structural element with respect to the bilayer normal. However, solids NMR methods are very demanding experimentally and have been restricted to relatively small proteins because of low resolution (*9*). Also, they are of limited suitability for the study of peripheral and membrane-anchored proteins because of the low surface hydration of typical bilayer preparations. The possibility of combining some of the advantages of solid- and liquid-state NMR measurements in a medium that provides a high hydration level and reasonably high resolution without the loss of structural data from angular parameters is intriguing.

The key to retaining sensitivity to angular parameters lies in preparing a membrane system with uniform orientation with respect to the magnetic field. Most molecules have weakly anisotropic magnetic susceptibilities and have a small natural tendency to orient in a strong field (*10*), and when they are constrained to behave cooperatively, as in liquid crystals, their anisotropies add, so that orientation tendencies become significant. Phospholipid bilayers are moderately anisotropic and naturally cooperative. At appropriate lipid to detergent ratios, it is possible to form phospholipid bilayer discs (bicelles) that orient cooperatively in the magnetic field and yet remain mobile enough to make high resolution NMR experiments possible (*11*, *12*).

† This work was supported by NIH Grant GM54160.
⊗ Abstract published in *Advance ACS Abstracts,* December 15, 1997.

S0006-2960(97)01779-0 CCC: $15.00
Published on Web 01/13/1998

In these oriented systems, it is possible to measure parameters containing angular information, such as the dipole interaction, which is often used for structure determination. For a pair of spin $^1/_2$ nuclei i and j, the splitting due to the dipolar coupling is

$$D_{ij} = -\frac{\gamma_i \gamma_j h}{2\pi^2 r^3}\left\langle \frac{3\cos^2\theta - 1}{2} \right\rangle \qquad (1)$$

where γ_i and γ_j are the gyromagnetic ratios for the spin $^1/_2$ nuclei, h is Planck's constant, r is the internuclear distance, and θ is the angle between the internuclear vector and the external magnetic field. In the above-mentioned systems, the value of D_{ij} is further scaled down by rapid internal motions and overall motions related to the degree of order of the bilayers. The broken brackets denote a time average over motions with time scales short compared to the reciprocal maximum splitting. It is clear from eq 1 that the dipolar coupling is a source of dynamic and structural information through its dependence upon θ, r, and the motional averaging of these quantities. In solution, rapid isotropic tumbling effectively averages the angular part of the above function to zero. The distance dependence can still be measured, but only indirectly, through relaxation processes (NOEs). In oriented systems, the dipolar coupling can be measured directly to obtain either angular or distance data. In our cases the distances (r) are treated as fixed parameters determined by chemical bonding and angular parameters are extracted.

It is possible to obtain additional information on the orientational properties of molecules by measuring chemical shift anisotropy effects. The chemical shift observed in an oriented system can be expressed as

$$\langle \delta_{obs} \rangle = \frac{1}{3}(\delta_{11} + \delta_{22} + \delta_{33}) + \langle \delta_{an} \rangle \qquad (2)$$

where δ_{ii} are the diagonal elements of the shift tensor. The anisotropic component of the observed shift, δ_{an}, displays an angular dependence similar to that of D_{ij}:

$$\langle \delta_{an} \rangle = -\frac{2}{3}\sum_{ij} \delta ij \left\langle \frac{3\cos\theta_i \cos\theta_j - k_{ij}}{2} \right\rangle \qquad (3)$$

where θ_i defines the instantaneous orientation of the ith molecular axis with respect to the director (a unit vector defining the preferred orientation of the molecules), δ_{ij} are the elements of the chemical shift tensor in the molecular frame, k_{ij} is the Kronecker delta, and broken brackets again denote a time average.

Previous studies have investigated the possibility of reconstituting integral and peripheral membrane proteins into bicelles and have reported varying degrees of success depending on the systems studied (*12*−*14*). The actual peptides studied here are derived from the N-terminal sequence of human ADP-ribosylation factor 1 (ARF1). ARF1 is a relatively small (21 kda) GTP binding protein that plays an important role in membrane trafficking (*15*). It is an N-myristoylated GTP/GDP switch protein. The lipid modification is essential for activity, and the GTP-bound form associates with the membrane more strongly than the GDP-bound form. In addition to the acyl chain, ARF1 has

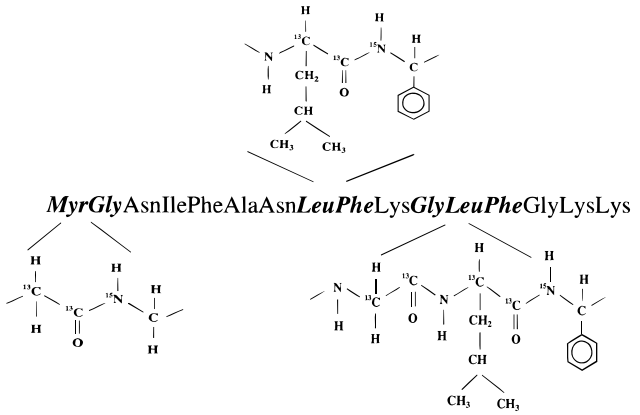

FIGURE 1: Labeling scheme for the 15 amino acid peptide (Myr15). Expanded regions show the exact positions of the ^{13}C and ^{15}N labels.

an N-terminal amphipathic helix that is believed to be involved in the association with the membrane (*16*, *17*). The X-ray structure of the nonmyristoylated, GDP-bound form of ARF1 is known (*18*). Although this provides a great deal of structural data on ARF1, it is not clear how the switch works, how the myristoyl chain is bound, and how the N-terminal amphipathic helix might interact with the membrane. NMR methods can in principle contribute to answering these questions. In these early applications of our new methods we chose to work with just N-terminal peptides rather than the whole protein. Some studies with short, N-myristoylated peptides have been conducted using electron spin resonance (ESR) and ^2H NMR spectroscopy, but these fall short of a true structural characterization (*19*). However, with the structural details available from NMR methods, work on even isolated terminal sequences should contribute to our understanding of ARF1−membrane interactions.

In the work to be presented, several N-myristoylated peptides of differing lengths were synthesized and studied. The shortest one is only three amino acids long (Myr3) and it could be incorporated into bicelles in large quantities, up to a lipid to peptide mole ratio of 20. This makes it a good test sample for new NMR techniques. Out of the longer peptides that were studied, a 15 amino acid long fragment (Myr15) behaved most favorably in oriented bicelles; at a lipid to peptide mole ratio of 60, the degree of orientation for the bicelles was highly homogeneous. This peptide includes the full N-terminal amphipathic helix (residues 1−11) and a few extra amino acids that are a part of a loop in the crystal structure. This peptide was the object of the most extensive structural studies. Some studies were also carried out on a 9 amino acid long peptide (Myr9), which lacks residues from the loop region and can be incorporated into the bicelle system only in small amounts.

The peptides were selectively ^{13}C- and ^{15}N-labeled at specific positions. Since the focus is on the angular dependence, the averages denoted by the brackets in eqs 1 and 3 have to be accurately described and for this it is useful to have at least three labeled sites in each rigid structural element of the molecule. The peptide plane can be considered to be such a rigid element with the ^{15}N amide nitrogen, the ^{13}C α-carbon, and the ^{13}C carbonyl carbon providing suitable labeling sites. The Myr15 peptide was labeled at four different peptide bonds (Figure 1).

MATERIALS AND METHODS

Peptides. The N-myristoylated 3 amino acid peptide (Myr3, Myr-GNI) was synthesized with labels introduced in the amide bond between the lipid chain and the first glycine using standard solution methods (*20*). The carboxyl end was left as a methyl ester, since for such a short peptide the charge of the end residue might have dominated its behavior at the membrane surface. The labeled glycine ([^{15}N]Gly) and the labeled myristic acid ([1,2-$^{13}C_2$]Myr) were purchased from Isotec Inc. (Miamisburg, OH).

The N-myristoylated 9 amino acid peptide (Myr9, Myr-GNIFANLFK) was synthesized using an Fmoc-Lys(Boc)-Wang resin purchased from Advanced ChemTech (Louisville, KY). First, labels were introduced only in the amide bond between the lipid chain and the first glycine. A second peptide was also synthesized with labels in two amide bonds, the one between the lipid chain and Gly_2 and the one between Leu_8 and Phe_9. The labeled amino acids ([^{15}N]Gly, [1,2-$^{13}C_2$]Leu, and [^{15}N]Phe) and the labeled myristic acid ([1,2-$^{13}C_2$]Myr) were purchased from Isotec Inc. (Miamisburg, OH). The Fmoc-protected forms of the labeled amino acids were synthesized according to standard procedures (*21*). The peptide was then prepared based on standard peptide synthesis procedures (*22*) and was purified by reverse-phase HPLC on a Vydac C18 preparative column with a gradient of 60−100% methanol in water, 0.1% TFA.

The N-myristoylated 15 amino acid peptide (Myr15, Myr-GNIFANLFKGLFGKK) was contract-synthesized and purified by J. Crawford of the Keck Biotechnology Laboratory at Yale University. Labels were introduced in four amide bonds, the one between the lipid chain ([1,2-$^{13}C_2$]Myr) and Gly_2 ([^{15}N]Gly), the one between Leu_8 ([1,2-$^{13}C_2$]Leu) and Phe_9 ([^{15}N]Phe), and the one between Leu_{12} ([1,2-$^{13}C_2$]Leu) and Phe_{13} ([^{15}N]Phe) and at Gly_{11} ([1,2-$^{13}C_2$]Gly), but here no ^{15}N was included. Sources for labeled materials were as indicated for the other peptides above.

Bicelle Preparation. DMPC/DHPC and DMPC/CHAPSO bicelles have been extensively described and characterized (*11*). Here only those details important to understanding the experiments are summarized. DMPC (L-α-dimyristoylphosphatidylcholine) and CHAPSO (3-[(cholamidopropyl)dimethylammonio]-2-hydroxy-1-propanesulfonate) were purchased from Sigma (St. Louis, MO). DHPC (L-α-dihexanoylphosphatidylcholine) was purchased from Avanti Polar Lipids (Birmingham, AL). Dispersal of mixtures of these lipids in aqueous buffer results in discoidal bilayerlike structures (bicelles) that orient with their normal perpendicular to the field when placed in a magnet. The use of lanthanide ions to achieve parallel orientation of the bilayer with respect to the magnetic field has been suggested as a means to improve resolution in many systems (23). Preliminary experiments with lanthanide-doped bicelles for our surface-associated fragments did not show the expected improvement, possibly because of interactions between the paramagnetic lanthanide ions and the studied peptide. Hence, bicelles that orient with their bilayer normal perpendicular to the magnetic field were used in this work.

For DMPC/DHPC bicelles the lipid composition used was DMPC:DHPC 2.8:1 mole ratio, 25% w/v. For DHPC/CHAPSO bicelles the lipid composition used was DMPC:CHAPSO 3:1 mole ratio, 30% w/v. All bicelle samples were buffered at pH 7 with a total buffer and salt concentration of 100 mM. An isotropic micelle phase was also prepared using lysophosphatidylcholine (LPC) to provide a chemical shift reference for the measurement of δ_{an}.

The peptides were reconstituted in the bicelles according to a method previously described (*14*). Attempts to incorporate Myr3 into DMPC/DHPC bicelles resulted in disordered preparations, but it could be reconstituted into DMPC/CHAPSO bicelles with a typical lipid to peptide mole ratio of 20. For Myr9, the typical lipid to peptide mole ratio was 400; any further increase in peptide concentration would disturb the bicelle orientation. Myr9 could also only be reconstituted into DMPC/CHAPSO bicelles. For Myr15, the typical lipid to peptide mole ratio was 60−100; a further increase in peptide concentration was not tested because of limited quantity of available peptide. Myr15 could be reconstituted into bicelles with either DHPC or CHAPSO as a detergent. For the isotropic samples Myr3, Myr9, and Myr15 were reconstituted by simple mixing (0.25 mM LPC solution, with a LPC:peptide ratio of around 100).

CD Spectroscopy. Preliminary characterization of the secondary structure of Myr9 and Myr15 was carried out using circular dichroism (CD) spectroscopy. Spectra were obtained on an Aviv 62DS spectrometer in a quartz cuvette of 0.1 cm path length. The measurements were done at 25 °C with a 5 s integration time and a 0.5 nm step size. The spectra were collected in 10 mM phosphate buffer with 1% total lipid concentration of DMPC:DHPC, mole ratio of 1:2, and 250 μM peptide concentration. Spectra of the peptide-free micelle solution were used to correct for background lipid absorbance and scattering.

NMR Spectroscopy. It is useful to factor out the effects of bicelle order from the motional averaging in eqs 1 and 3 to independently assess these contributions. ^{31}P NMR as applied to the phosphate sites in the bilayer lipids was used to accomplish this after reconstitution of the peptides. By measuring δ_{an} for the lipid headgroup, the degree of order for the bilayer can be calculated:

$$S_{\text{bilayer}} = \left\langle \frac{3\cos^2\alpha - 1}{2} \right\rangle = \frac{\delta_{\text{an}}}{\delta_{90^\circ,\ \text{powder pattern}} - \delta_{\text{iso}}} \quad (4)$$

where α is the angle between the instantaneous and average symmetry axis of the bilayer disks. S_{bilayer} ranged from −0.48 to −0.72 in the systems studied. All ^{31}P spectra were collected on a GE Omega-300 spectrometer using a Bruker QNP probe. Proton decoupling was accomplished using GARP-1 with a 90° pulse width of 30 μs on the decoupling channel. The temperature for optimal orientation and order was determined to be 45 °C on the basis of ^{31}P measurements.

Most of the ^{13}C spectra of peptides were collected on a 500 MHz Varian Inova spectrometer using a ^{13}C-detect triple resonance probe specifically modified to handle higher power (30−40 W) on the proton channel for extended periods of time. A standard variable-temperature controller was utilized for the temperature settings. Samples were generally incubated in the magnet for 15−30 min prior to acquisition to ensure uniform orientation and temperature. Typical experimental parameters were 7 μs, 90° pulse width for ^{13}C; 30 μs, 90° pulse width on the decoupler channel for ^{1}H (proton decoupling was accomplished using WALTZ-16);

90 μs, 90° pulse width on the second decoupler channel for ^{15}N (nitrogen decoupling was done using GARP-1); 60−80 ms acquisition time; and a relaxation delay of 1.5−2.0 s. All 1D ^{13}C spectra were recorded utilizing NOE enhancement. Depending on sample concentration, the time required for a 1D ^{13}C spectrum was less than half an hour for Myr3 and was between 8 and 24 h for Myr15. Chemical shifts were referenced indirectly to tetramethylsilane (TMS).

For suppressing the background signals from the lipids, 1D-INADEQUATE experiments (*24*) were run. The experimental parameters were similar to those of a 1D ^{13}C spectrum except that a double quantum filter sequence was inserted with the delays adjusted approximately for the expected size of the couplings ($^1/_4(D + J)$; 1.25 ms for a 200 Hz coupling).

To determine the relative sign of $^1D_{CN}$ and $^2D_{CN}$ for Myr3, a 2D ^{13}C−^{13}C double quantum filtered correlated spectrum (DQF-COSY) was acquired. This measurement was done on a Bruker AM500 spectrometer using a ^{13}C detect double-resonance probe with a 90° pulse width of 9.5 μs and 20 W decoupling power during acquisition (90 ms). In the indirect dimension a sweep width of 1500 Hz was used and the carrier position was optimized so that the carbonyl and the α-carbon peaks would not fold onto each other. Sixty-four complex t_1 points were acquired leading to 24 Hz/point resolution in the indirect dimension.

δ_{an} for the ^{15}N amide nitrogen of Myr3 was determined using off-resonance nitrogen continuous-wave (CW) decoupling and observing the collapse of the ^{13}C-^{15}N coupling in the ^{13}C spectrum as a function of the carrier frequency for ^{15}N. The oriented and isotropic samples were run immediately after one another to minimize the error from the drift of the magnetic field.

Direct ^{15}N observe experiments were run on a wide-bore 500 MHz Varian Inova spectrometer using an H-X-Y triple-resonance 4 mm Chemmagnetics MAS probe in a double-resonance configuration. The spectra were obtained with a spin-lock tangent ramped cross-polarization sequence (*25*) on static samples. Typical experimental parameters were 18 μs, 90° pulse width; 5 ms, mix for Myr3, and 0.5 ms, mix for Myr15; 2 s, relaxation delay; and 25 ms, acquisition time, at 45 °C. ^{1}H decoupling was accomplished with WALTZ-16 (90° pulse width of 20 μs) during acquisition. A total of 1024 scans were acquired for Myr3 and several thousand scans were acquired for Myr15 on sample volumes of around 100 μL. The ^{15}N chemical shifts are referenced to [^{15}N]ammonium nitrate in aqueous nitric acid (*26*).

Data Analysis. Processing of the data sets was done with Felix95 (Biosym Technologies). Extraction of the coupling constants from INADEQUATE spectra was done using a Monte Carlo-based Bayesian parameter estimation method (*27*). For the large couplings simply measuring the peak to peak separation proved adequate.

Because of the wobbling of the bilayer disks and the complex internal motions of the anchored peptides, the measured parameters are affected by extensive dynamic averaging. The motion of the disks scales all the anisotropic interactions uniformly by the factor $S_{bilayer}$ (see NMR Spectroscopy), but the complex motions of the surface-associated molecules cannot be taken into account by just a scaling factor. A simple approach is to represent the averaging of the anisotropic interactions by an order matrix (S_{ij}) (*28*−*30*). For a molecule with coordinates defined in an arbitrary Cartesian system, the elements of the order matrix are

$$S_{ij} = \left\langle \frac{3\cos\theta_i \cos\theta_j - k_{ij}}{2} \right\rangle \quad (5)$$

These are the same averages that occur in the expression for δ_{an} (eq 3).

The angular factor in the dipolar splitting expression can also be expressed in terms of the same order matrix elements:

$$\left\langle \frac{3\cos^2\theta - 1}{2} \right\rangle = \cos^2\varphi_x(-S_{yy} - S_{zz}) + \cos^2\varphi_y S_{yy} + \cos^2\varphi_z S_{zz} + 2\cos\varphi_x \cos\varphi_y S_{xy} + 2\cos\varphi_x \cos\varphi_z S_{xz} + 2\cos\varphi_y \cos\varphi_z S_{yz} \quad (6)$$

Here φ_i is the angle of the internuclear vector relative to the ith molecular axis. The order matrix is symmetric and traceless, so there are only five independent parameters. These can be determined from experimental data if a sufficient number of different δ_{an} and D_{ij} values can be measured.

By diagonalizing the order matrix, it is possible to reduce the order parameter description to a principal order parameter ($S_{z'z'}$) and an asymmetry parameter [$\eta = (S_{x'x'} - S_{y'y'})/S_{z'z'}$]. The transformation matrix that accomplishes this diagonalization contains the orientational information relating the principal averaging frame to the initial molecular frame.

For the calculations, the starting molecular geometry of the N-terminal segment was based on the X-ray structure of human ARF1 (*18*). The nearly helical X-ray structure of this region was modified to be a perfect right-handed helix using molecular mechanics minimization methods [all-atom force field of AMBER 4.1 (1995, University of California, San Francisco)]. The values of the peptide carbonyl ^{13}C and the amide ^{15}N shift tensor elements and the orientation of the shift tensors were based on literature values (*31*), and dipolar coupling constants were calculated assuming a rigid peptide framework as deduced from the minimized structure.

A C program based on the Fortran program ORDERTEN (*32*) performed a quasi random search (*33*) of the 5D space of physically allowed values of the order matrix elements to find those that reproduce the measured NMR data within experimental error. As discussed above, five or more independent measurements from each rigid unit may be required to provide complete evaluation of all elements. However, it is often experimentally difficult to get more than three pieces of data from a rigid segment of a peptide. Also, frequently only the absolute value of the dipolar couplings can be determined. Performing the order matrix calculation on such an underdetermined system will yield a distribution of order parameters and a collection of vectors defining possible directions of highest order. To facilitate the visualization of the distribution of vectors consistent with the measured data, a mapping technique was employed. The equal area pseudocylindrical Sauson Flamsteed projection (*34*) is well-suited for the purpose. The simple transformations $x = R\lambda \cos\phi$ and $y = R\phi$ are employed, where ϕ is the latitude and λ is the longitude. Calculations of the longitude and latitude can be done from the Cartesian coordinates of any vector. It is important to keep in mind

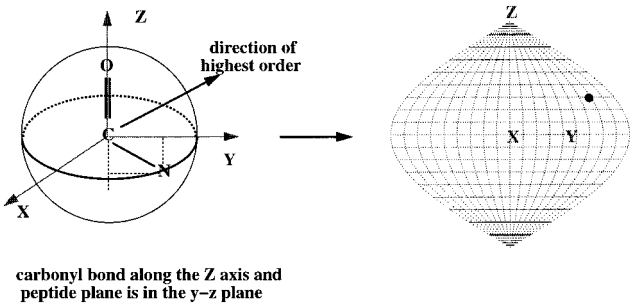

FIGURE 2: Axes definition for the Sauson Flamsteed projection showing allowed orientations for the direction of the highest order. The dot on the right diagram corresponds to the point of intersection of the director with the surface of the sphere on the left.

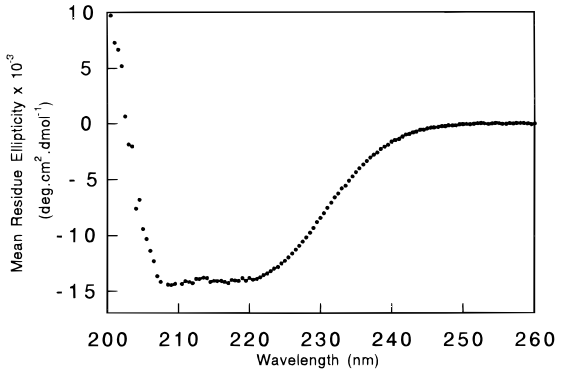

FIGURE 3: CD spectra of Myr15 in DMPC/DHPC micelles at 25 °C in pH 7 phosphate buffer. The ordinate represents mean residue molar ellipticity.

that the maps are only meaningful if the molecular frame is defined with respect to the frame of the mapping. For all maps presented in this paper a separate molecular frame is used for each peptide bond such that the carbonyl bond of the amide plane is along the *z* axis and the C−N bond is in the *y*−*z* plane (Figure 2).

RESULTS

Before beginning a more detailed structural analysis, it is useful to know the preferred secondary structure type of the peptides chosen. To accomplish this we examined the CD spectrum of Myr9 and Myr15 in a micelle solution. The peptides are not soluble in water. On the basis of these spectra, both peptides are definitely structured. Myr9 shows some helical tendencies, while for Myr15 the broad minima between 205 and 220 nm are consistent with a significant part of the peptide being helical (Figure 3). The mean residue molar ellipticity at 220 nm (*35*) shows the presence of ∼45% α-helix in the Myr15 peptide. Although the CD data can give some general information on the secondary structure of the peptides, it cannot provide details of the structure, such as the orientation of the hydrophobic face of the helix with respect to the bilayer normal, nor can it give any dynamic information. These questions can be approached using NMR spectroscopy in magnetically oriented bicelles.

One might expect to extract a large amount of data from the carbonyl region of the ^{13}C spectrum since the shielding anisotropy of a carbonyl carbon is large and $\langle\delta_{an}\rangle$ can be measured with high precision. These signals should also be split by dipolar couplings to the neighboring ^{13}C α-carbon and, in some cases, to the ^{15}N amide nitrogen of the sequential residue. Figure 4 compares a ^{13}C spectrum of Myr15 in an isotropic micelle phase (panel a) to one in an oriented bicelle phase (panel b). It is clear that upon orientation of the bilayer disks the resonances become widely dispersed due to chemical shift anisotropy effects, and splittings change due to the fact that the dipolar interactions no longer average to zero. The spectral resolution is excellent. Note that there are two identical Leu-Phe segments at residues 8−9 and residues 12−13. Although the carbonyl ^{13}C signals from these amide bonds are closely grouped in the isotropic phase, they differ by around 20 ppm in the oriented phase. Hence, orientation rather than residue type dominates these shifts.

To make use of the splittings and offsets measured from spectra such as the one in Figure 4b, the resonances need to be assigned. For Myr3 and Myr9 peptides the assignment is not a problem, since Myr3 contains only one labeled segment between the lipid chain and Gly_2 and Myr9 contains only one additional segment. The new set of peaks for Myr9 were therefore assigned to Leu_8. However, assignment for Myr15 is a challenging problem. While resolution is good, the assignment is not easy when focusing on just the carbonyl region. The chemical shifts themselves are of little aid in identifying residue types because they are dominated by orientational effects. However, chemical shifts of α-carbons can assist in the assignment process. They have a reasonably large chemical shift dispersion due to residue type and display smaller chemical shift anisotropy effects. Two-dimensional ^{13}C-INADEQUATE experiments can connect carbonyl carbons with the neighboring α-carbons through their common double quantum coherence. For our simple cases, the 1D analogues of this experiment are often adequate because pairs of resonances with equal intensity and equal splittings can often be identified. These experiments also very effectively eliminate the natural-abundance ^{13}C resonances from the lipid because these sites only rarely occur as coupled pairs, thus making the labeled α-carbons of the peptide observable. Figure 5 illustrates both the 1D carbon spectrum of Myr15 in oriented bicelles and the 1D-INADEQUATE spectrum. Since the sensitivity for a double quantum filtered experiment is half that of a simple 1D acquisition and there are some relaxation losses during the preparation period, only the sharper peaks of the peptide are readily visible. On the basis of the isotropic α-carbon shifts determined from peptides in LPC micelles and the pairing established on the similarity of antiphase couplings, the upfield, broader carbonyl doublet (170 ppm) is identified as one of the leucines, while the sharper downfield doublet of doublets is identified as the ^{13}C carbonyl of the lipid chain (Myr). The [1-^{13}C]Myr−[^{15}N]Gly coupling is passive in this experiment, leading to an in-phase doublet, while the [1-^{13}C]-Myr−[2-^{13}C]Myr coupling is active, resulting in an antiphase doublet. Although both Leu_8 and Leu_{12} have an ^{15}N neighbor, no nitrogen coupling can be measured for the upfield peak. The observed splittings are always the sum of the scalar and the dipolar couplings, so if these two couplings happen to be equal but have opposite sign there will be no measurable splitting. We believe this happens for one of the Leu-Phe pairs.

An examination of the spectrum in Figure 4b shows that the broad doublet centered at 187 ppm and a set of peaks

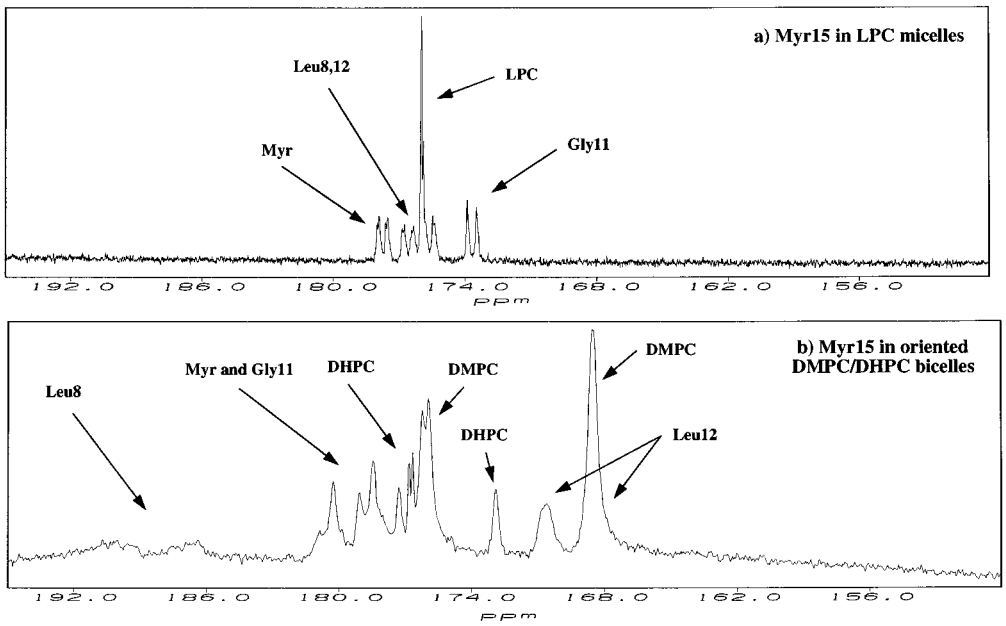

FIGURE 4: Comparison of the isotropic and oriented ^{13}C spectra of Myr15. Only the carbonyl region is shown. Upon orientation the signals shift due to anisotropic averaging of the chemical shift tensor and the couplings change due to the presence of residual dipolar couplings. (a) Proton-decoupled ^{13}C spectrum of Myr15 in isotropic LPC micelles. (b) Proton-decoupled ^{13}C spectrum of Myr15 in magnetically oriented DMPC/DHPC bicelles.

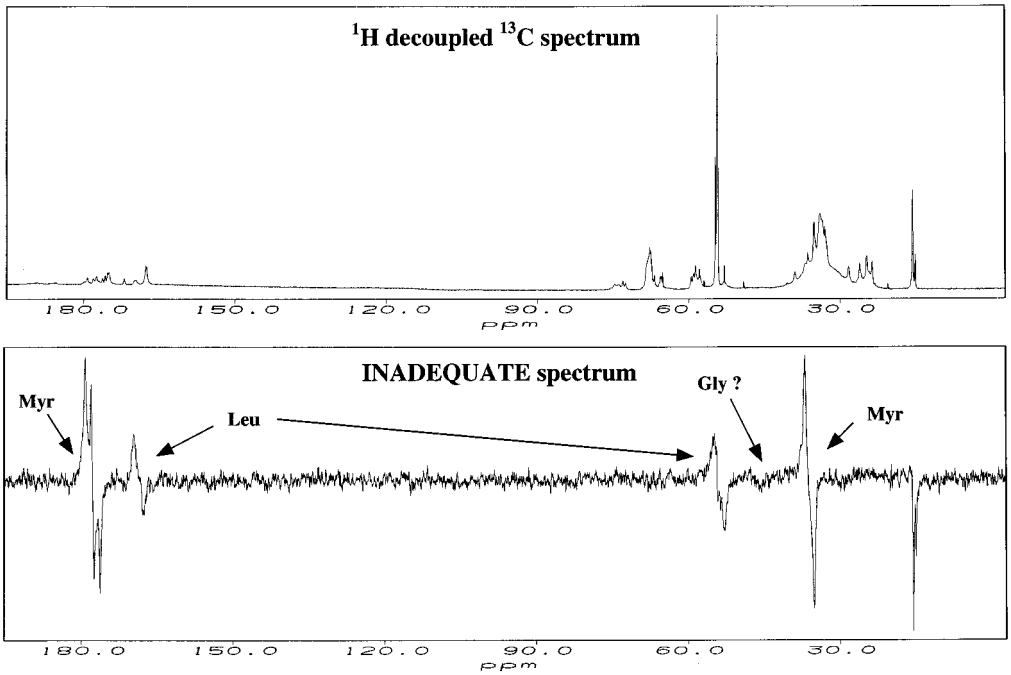

FIGURE 5: Proton-decoupled ^{13}C spectrum and ^{13}C INADEQUATE spectrum of Myr15 in DMPC/DHPC bicelles (2.8:1, 25% w/v). Through double-quantum filtering the INADEQUATE experiment eliminates the lipid background and correlates coupled $^{13}C-^{13}C$ pairs. Arrows indicate assignments based on this experiment.

under the carbonyl signal of Myr at 178 ppm remain to be assigned. These must be from either Gly_{11} or the remaining Leu. Since Gly_{11} has the only ^{13}C carbonyl that does not have an adjacent ^{15}N neighbor, nitrogen decoupling might be employed to distinguish between these possibilities. Figure 6 compares the carbonyl region of the proton-decoupled carbon spectrum and a proton- and nitrogen-decoupled carbon spectrum of Myr15 in oriented bicelles. The most downfield doublet is affected by ^{15}N decoupling, so these peaks must be from one of the labeled Leu carbonyls and not from Gly_{11}.

It is still necessary to distinguish between Leu_8 and Leu_{12}. This can be accomplished by comparison to results from the Myr9 peptide. The fact that in the Myr9 peptide Leu_8 has a downfield shift in a comparable DMPC/CHAPSO preparation suggests that the downfield Myr15 peak should be assigned to Leu_8 and the most upfield doublet should be assigned to Leu_{12}.

Upon completion of the full assignment of the carbonyl peaks of Myr15, the dipolar couplings and the anisotropic component of the observed shifts (δ_{an}) were determined. δ_{an} for the ^{13}C carbonyl carbons were easily measured by

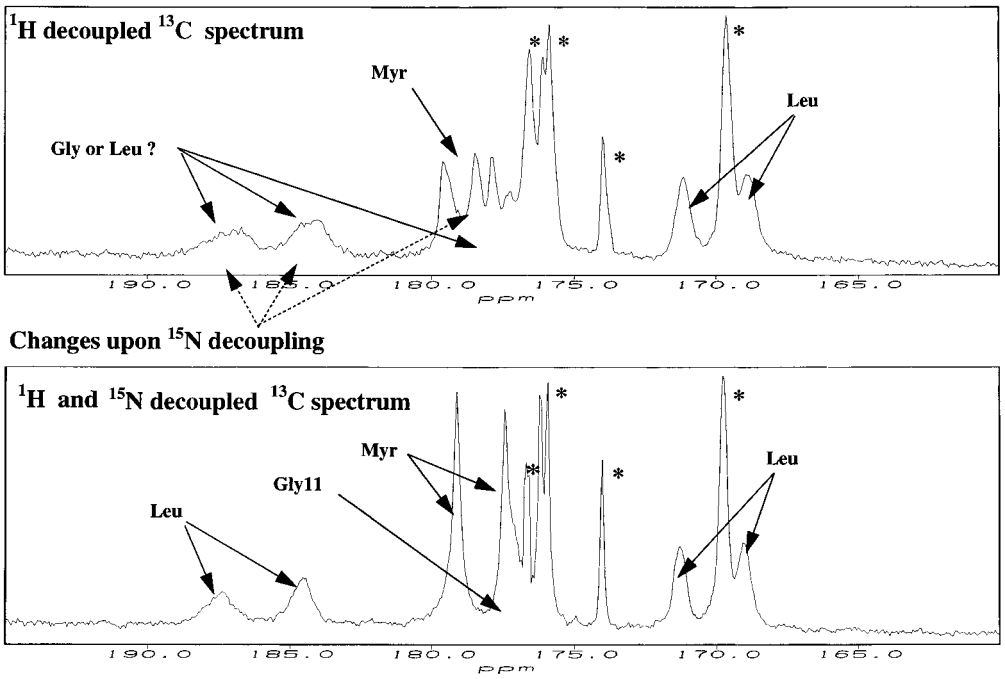

FIGURE 6: Comparison of the ^{1}H-decoupled and the ^{1}H- and ^{15}N-decoupled ^{13}C spectrum of Myr15 in DMPC/DHPC bicelles (2.8:1, 25% w/v). (The asterisks indicate ^{13}C peaks arising from the lipid matrix and only the carbonyl region is shown.) Arrows indicate assigned sites; dashed lines indicate sites affected by ^{15}N decoupling.

comparison of the chemical shifts in the oriented sample to isotropic shifts measured in a LPC micelle (Figure 4). Attempts were also made to measure δ_{an} for the ^{15}N amide nitrogens in Myr15, but only a broad line (200 Hz) could be observed in the proton-decoupled nitrogen spectrum, which could results from the overlap of two or maybe all three expected lines. δ_{an} for this broad signal is positive and is between 5 and 15 ppm.

Determination of the dipolar couplings is a little more involved. For Leu_{12} and Myr the $^{CC}(J + D)$ and the $^{CN}(J + D)$ values were determined from the INADEQUATE spectrum using a Monte Carlo-based Bayesian parameter estimation method (*27*). The absence of $^{CN}(J + D)$ for Leu_{12} was confirmed by ^{15}N decoupling and ^{15}N-edited experiments. The $^{CC}(J + D)$ of Leu_8 was measured from a 1D carbon spectrum. The small ^{13}C−^{15}N coupling for Leu_8 could be estimated on the basis of the narrowing of the lines upon ^{15}N decoupling. The ^{13}C−^{13}C coupling in Gly_{11} was estimated by comparison of the peak at 178 ppm (nearly under Myr) in the 1D carbon and the 1D ^{15}N-decoupled carbon spectrum. In each case the value of D_{ij} was obtained by assuming that it had either added to or subtracted from the known scalar coupling values to produce the observed splitting. This generates two possible D_{ij} values with different signs for each nuclear pair except for those for which the splittings are zero or very close to zero. In these cases a unique value of D_{ij} can be determined. Combining the measured dipolar couplings for each peptide bond yields a certain number of possible sign sets for each amide bond; Myr has four possible sign sets, while all the other rigid units have only two.

Reduction in the number of possible sign sets can greatly accelerate the search for allowed structures. One way to accomplish this is to determine at least the relative signs of some dipolar couplings in a set. Since Myr3 could be incorporated into the bicelle system at high concentration,

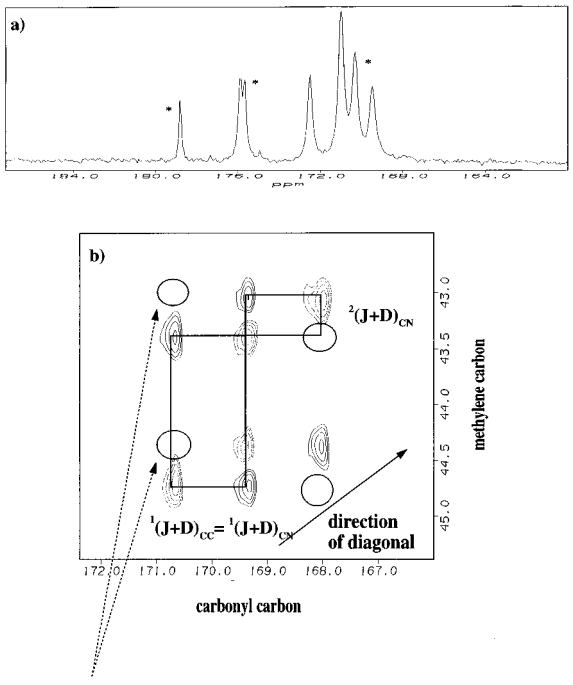

FIGURE 7: (a) Carbonyl region of the proton-decoupled ^{13}C spectrum of Myr3 in magnetically oriented DMPC/CHAPSO bicelles. (The asterisks indicate ^{13}C peaks arising from the lipid matrix.) (b) The downfield cross peak of the ^{13}C−^{13}C DQF-COSY spectrum acquired on Myr3 in oriented DMPC/CHAPSO bicelles. On the basis of the position of the missing peaks, it is possible to determine the relative sign of $^1D_{CN}$ and $^2D_{CN}$.

and the achieved resolution was very good (40 Hz line width), it was possible to determine the relative signs of the one- and two-bond ^{13}C−^{15}N dipolar couplings using a 2D ^{13}C−^{13}C DQF-COSY experiment. Multiples in normal homonuclear COSY spectra give cross peaks with compo-

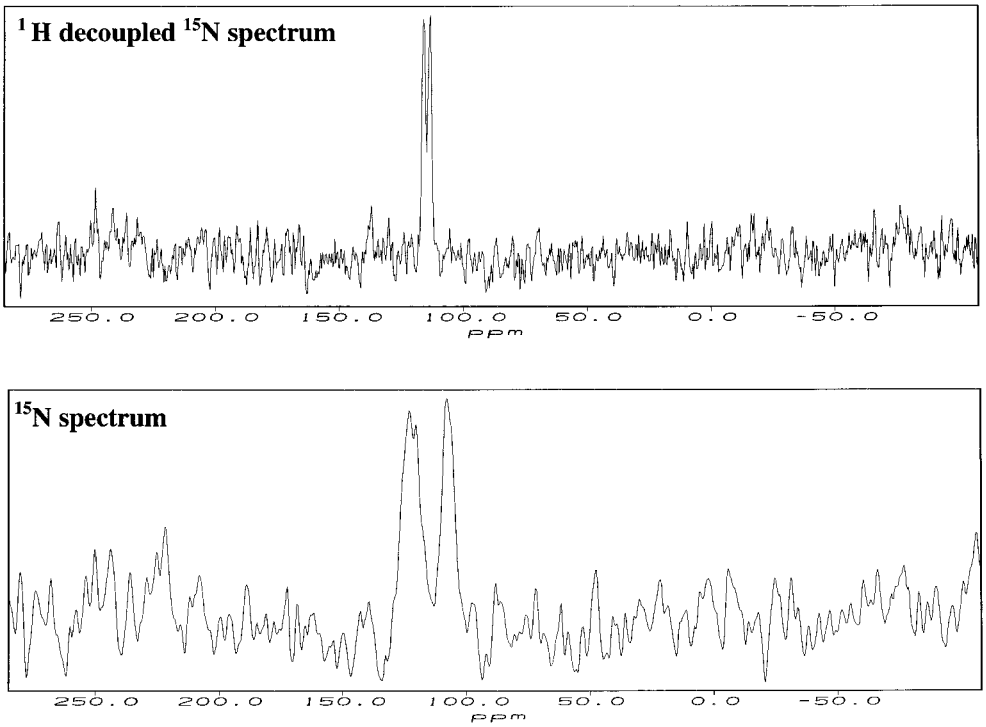

FIGURE 8: Comparison of the ^{1}H-decoupled and the ^{1}H-coupled ^{15}N spectrum of Myr3 in DMPC/CHAPSO bicelles (3:1, 30% w/v).

Table 1: Summary of Experimental Data[a]

amide plane	data	Myr3	Myr9	Myr15
Myr-Gly$_2$	$^1D_{CC}$	-223 or $+123 \pm 20$	-50 ± 25	-277 or $+177 \pm 20$
	$^1D_{CN}$	-160 or $+187 \pm 20$	-116 or $+143 \pm 25$	-131 or $+161 \pm 20$
	$^1D_{NH}$	-655 or $+845 \pm 50$	not measured	not measured
	$^2D_{CN}$	-32 or $+48 \pm 20$	not resolvable	not resolvable
	δ_{an} (^{13}C)	-5.7 ± 1.0	-1.9 ± 1.0	0.0 ± 0.5
	δ_{an} (^{15}N)	$+6.0 \pm 3.0$	not measured	not measured
Leu$_8$-Phe$_9$	$^1D_{CC}$	N/A	-276 or $+176 \pm 50$	-550 or $+450 \pm 50$
	$^1D_{CN}$	N/A	not resolvable	$+15 \pm 50$
	δ_{an} (^{13}C)	N/A	not measured	$+12.3 \pm 1.0$
Gly$_{11}$	$^1D_{CC}$	N/A	N/A	-265 or $+165 \pm 50$
	$^1D_{CN}$	N/A	N/A	N/A
	δ_{an} (^{13}C)	N/A	N/A	$+4.5 \pm 1.0$
Leu$_{12}$-Phe$_{13}$	$^1D_{CC}$	N/A	N/A	-296 or $+196 \pm 30$
	$^1D_{CN}$	N/A	N/A	$+15 \pm 30$
	δ_{an} (^{13}C)	N/A	N/A	-7.6 ± 0.5

[a] All couplings are in hertz and the anisotropic part of the chemical shifts are in parts per million.

nents correlating every line of one multiplet with every line of a connected multiplet. For a homonuclear three-spin system, half of these arise because the spin state of the passive spin is also perturbed by the 90° mixing pulse. When the passive spin is ^{15}N, however, and a homonuclear ^{13}C COSY spectrum is acquired, the ^{15}N spin is not affected and half the cross-peak components are missing. The position of these missing components identifies the relative sign of the one- and two-bond carbon−nitrogen couplings. This is illustrated in Figure 7, which shows one cross peak from the DQF-COSY spectrum. Since the ^{13}C cross peaks with identical spin states lie parallel to the diagonal, the two couplings have the same sign.

It was also possible to measure ^{15}N δ_{an} for Myr3 by using off-resonance nitrogen decoupling, and the $^1D_{NH}$ dipolar coupling could be determined by direct nitrogen observe experiments (Figure 8). All together, six independent measurements were done on the labeled amide fragment of Myr3; four of these involved dipolar couplings. When all the possible combinations for the signs of the dipolar couplings are taken into account, there are 16 possible sign sets for this peptide. This number was reduced to eight on the basis of the determined relative signs.

Myr9 is hard to study in the bicelles because of low concentration. Still, the one-bond carbon−nitrogen and carbon−carbon coupling and the anisotropic part of the chemical shift for the carbonyl carbons could be determined for the labeled Myr site. The ^{13}C−^{13}C dipolar coupling is close to zero, leading to only two possible sign sets. Table 1 summarizes the experimental data for all studied peptides.

DISCUSSION

As detailed in the Materials and Methods section, analysis of the dipolar coupling constants and chemical shift anisotropy data is based on an order matrix approach. In some

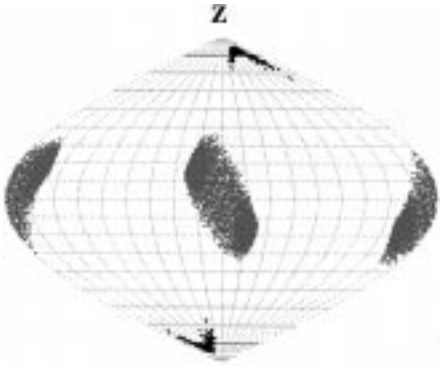

FIGURE 9: Possible orientations for the direction of highest order for Leu_8 (gray dots, center) and Leu_{12} (black dots, poles). For both amide bonds the molecular frame for the mapping is as described in Figure 2. The solutions for Leu_8 are consistent with a helix lying flat on the membrane surface. The solutions for Leu_{12} indicate that this part of the peptide cannot be a part of a surface-associated helix.

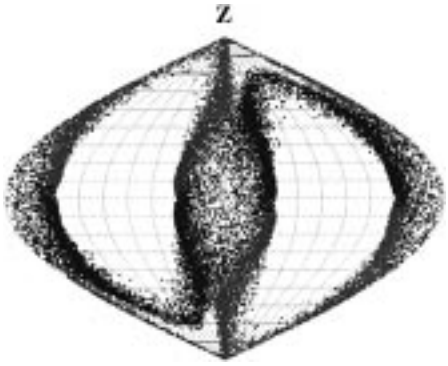

FIGURE 10: Possible orientation for the direction of highest order for Gly_{11}. The gray and black dots represent the two possible sign sets. The molecular frame for the mapping is as described in Figure 2. A considerable number of solutions are consistent with Gly_{11} being part of the same helix as Leu_8.

circumstances five independent pieces of data could be needed from each rigid $C_\alpha-C(O)-N$ peptide plane for the full evaluation of the order matrix. In practice, because of experimental limitations, one seldom achieves the goal of making five independent measurements and usually the acquired data is complicated by the existence of multiple sign sets. Nevertheless, lesser numbers of data can greatly restrict structural and motional models, and depending on the orientation of the studied fragment, in certain cases, a single experimental datum can restrict the possible direction of highest order to a very small range.

In Myr3 and Myr9 only the orientation of the amide bond between the myristic chain and Gly_2 was determined. For both peptides only one sign set gave solutions when all the acquired data were used. Out of the four peptide units of the studied Myr15 peptide, only in two cases are the experimental data sufficient to position them with respect to the bilayer with reasonable accuracy. These are the amide bonds between the two labeled leucines (Leu_8 and Leu_{12}) and the following phenylalanines. For both of these only one sign set gave solutions.

Figure 9 shows the acceptable directions of the bilayer normal with respect to the Leu8−Phe9 amide bond as described in Figure 2. Note that the normal is determined to be perpendicular to the axis along the carbonyl bond and to the plane of the peptide bond. This is consistent with a helical peptide lying flat on the surface of the membrane with the hydrophobic side chains extending into the membrane surface. Figure 9 also shows data on $Leu_{12}-Phe_{13}$. In this amide plane the orientation of the carbonyl bond is very different; it is close to being parallel to the bilayer normal, indicating that this part of the peptide cannot be a part of a surface associated helix. It is physically reasonable to assume that this carbonyl bond is pointing away from the bilayer, since this would position the hydrophobic aromatic ring of Phe_{13} close to the membrane surface. The data from Gly_{11} restrict the orientation of the bilayer normal to roughly a full circle that contains the C═O bond and the vector perpendicular to the amide plane (Figure 10). The gray and the black circles represent solutions from the two possible sign sets. A considerable number of orientations on this circle are consistent with Gly_{11} being part of the same helix as Leu_8. Hence a model emerges in which the central part of the helix (Leu_8) lies along the membrane surface. This could extend to Gly_{11} but it must deviate sharply at Leu_{12}. If residues 2−11 are treated as a rigid, perfect helix, the radical conformational difference of Leu_{12} cannot be modeled with only two dihedral rotations between Gly_{11} and Leu_{12}; however, only slight modifications are needed at Gly_{11} to allow this model.

The data for Myr of Myr15 is less conclusive; two out of the four sign sets give solutions, and the possible directions of highest order have a large spread. However, comparison of data from the amide bond between the lipid chain and Gly_2 for different length peptides is interesting. For Myr3 the direction of highest order can be determined to high accuracy (Figure 11a); the carbonyl bond is close to being perpendicular to the bilayer normal, so the C═O bond is close to being parallel to the membrane surface. The data for Myr9 and Myr15 are not so well determined (Figure 11b,c), but the series displays a monotonic trend that allows us to select solutions from one sign set of Myr15 as depicted (Figure 11c). If we assign the ^{15}N peak observed for Myr15 to the $MyrGly_2$ amide bond, the ^{15}N δ_{an} further restricts the allowed solutions to a region that is consistent with the C═O bond of the Myr being close to perpendicular to the bilayer normal. The assignment of the ^{15}N resonance is plausible since the Myr−Gly_2 amide bond consistently gives the sharpest signals and the Myr15 ^{15}N shift is near that of Myr3. Note, however, that the allowed solutions, near the center of the graph in Figure 11c, do not exactly overlap the solutions from Myr3, and so carbonyl orientation for these two peptides are not identical.

Figure 12 shows a plausible structure for Myr15 in the membrane environment that is consistent with all the observed data. A substantial part of the peptide is α-helical in a manner that is qualitatively consistent with the CD data. The most substantial departure is at the C terminus, where the $Leu_{12}-Phe_{13}$ amide bond is definitely not part of the helix, and subsequent residues may not be as well.

The order matrix calculations not only give structural information but also yield two order parameters that describe the motional averaging along the direction of highest order ($S_{z'z'}$) and the asymmetry in motion about this axis [$\eta = (S_{x'x'} - S_{y'y'})/S_{z'z'}$]. On the basis of the calculated results, the dynamic behavior of the segments in the Myr15 peptide is all similar. The axial order parameter ($S_{z'z'}$) for Leu_8 and Leu_{12} is 0.55 ± 0.15. The Gly_{11} solutions that are consistent

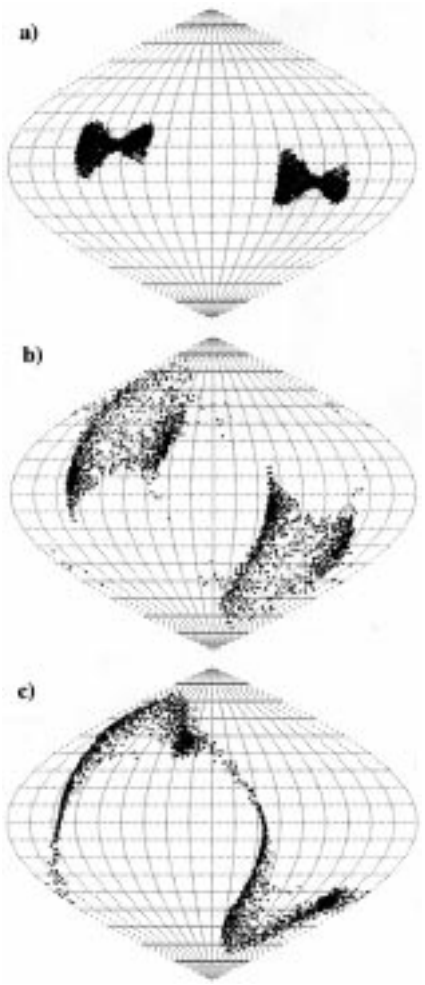

FIGURE 11: Possible orientation for the direction of highest order for the Myr segment in the three different peptides: (a) Myr3, (b) Myr9, and (c) Myr15. The molecular frame for the mapping is as described in Figure 2.

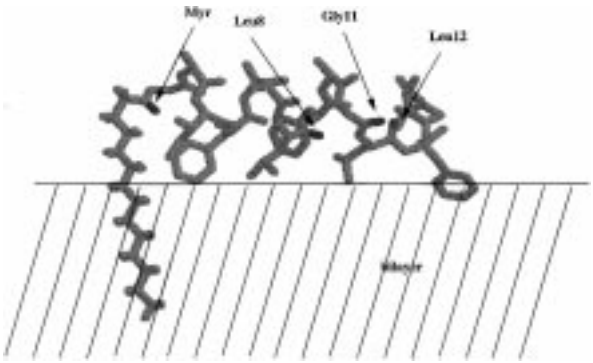

FIGURE 12: An orientation and structure of Myr15 at the bilayer surface that is consistent with the data. Arrows indicate sites where structural information was collected.

with an α-helix have an axial order parameter of 0.5 ± 0.3. For the Myr segment in all three peptides $S_{z'z'}$ is 0.4 ± 0.2. These order parameters are quite high and are close to the order parameters found for the backbones of lipids constituting liquid crystal bilayer membranes. This suggests the peptide to be fully associated with the membrane. Note, however, that line widths from resonances associated with various bonds are different, and the narrowest lines, those from the Myr−Gly_2 bond, correlate with the smallest order parameters. This suggests the existence of some internal motion in the peptide. The asymmetry parameters for the allowed solutions are more broadly spread ($|\eta| = 0.0-1.2$) and may not have the precision required for a detailed interpretation.

Relating the above model to the available data on the intact ARF1 protein is an interesting exercise. The N-terminal helix has been shown to be held by hydrophobic forces in a cleft of the unmyristoylated, GDP-bound form of ARF1 (*18*). In this case, the hydrophobic residues of the amphipathic helix are turned toward the inside of the protein, and the hydrophilic surface of the helix is exposed to the aqueous environment. Phe_{13} is positioned on the hydrophilic side and is exposed to solvent. The helix is actually characterized in the crystal structure as ending at residue 11 followed by a loop, but the geometry for Phe_{13} is nearly consistent with a simple extension of the helix. It is suggested that upon GTP binding the protein undergoes a conformational change that exposes the lipid chain (*17*). It is believed that although the hydrophobic insertion of the acyl chain into the bilayer is necessary, it is not sufficient to anchor the protein to the membrane (*36*). It is therefore possible that the conformational change upon GTP binding also exposes the hydrophobic surface of other parts of the protein so they can interact with the membrane; the N-terminal helix of ARF1 may be involved in this process.

In the model proposed here for the N-terminal helix fragment of ARF1 in the membrane environment, the amphipathic helix interacts with the bilayer surface with all the hydrophobic residues, including Phe_{13}, turned toward the membrane surface. The helix ends roughly at Gly_{11} with a more severe departure from helix geometry for Phe_{13}. On this basis, it is possible that upon membrane association there is a rather dramatic change in the orientation of the N-terminal helix. To test such a hypothesis, it will be necessary to study larger protein fragments and possibly the intact ARF1 protein.

The results presented here show considerable promise for using oriented sample NMR methodology on larger and more extensively labeled systems. Given the relatively high order parameters, the correlation time of membrane-anchored peptides and proteins studied in bicelles may be as much determined by the slow tumbling and wobbling motions of the bilayer disks as by the size of the peptide itself. The line width of the ^{13}C signal from the labeled carbonyl in the myristoyl chain, for example, hardly changes from a myristoylated glycine to the Myr15 peptide (around 40−50 Hz). Line widths of the other carbonyl signals within a single peptide such as Myr15, however, do vary substantially (50−175 Hz). This suggests that local motion and the specific orientation of the particular segment, as opposed to simple size of the peptide, may dominate variations in line width. So, extending the peptide might be done at minimal cost in increased line width. The $^1(J + D)_{CC}$ and $^1(J + D)_{CN}$ values are expected to be in the 0−400 Hz range, so with average line widths of even 100 Hz, the resolution will be acceptable.

The results also offer promise for work with extensively or even uniformly labeled peptides. While in isotropic phase the chemical shift dispersion of carbonyl peaks is around 10 ppm, in the oriented phase this can extend up to 40 ppm because of orientation-dependent chemical shift anisotropy effects. Correlating the well-resolved carbonyl peaks to the neighboring α-carbon peaks can be a reasonable starting

point for assignments. Further utilization of $^{13}C(=O)-^{15}N$ couplings and 2D carbon−nitrogen correlation experiments can be used to carry assignments from residue to residue along the peptide backbone. Nitrogen chemical shifts were used to a minimal extent in the analysis presented here, but their utility has been extensively documented by work of others (*7*, *9*). The $^{13}C-^{15}N$ correlation experiments would naturally produce these data.

ACKNOWLEDGMENT

We thank M. Andrec for his help, comments, and advice on the order matrix calculations and the map projection and for performing the Bayesian parameter estimation. We also thank L. Fisher for advice on the peptide synthesis and purification and S. Dalal for her help with the CD measurements.

REFERENCES

1. Shinitzky, M. (1993) *Biomembranes*, VCH, New York.
2. White, S. H. (1994) *Membrane Protein Structure, Experimental Approaches*, Oxford University Press, New York.
3. Schertler, G. F. X., Villa, C., and Henderson, R. (1993) *Nature 362*, 770−772.
4. Pickot, D., Loll, P. J., and Gravito, R. M. (1994) *Nature 367*, 243−249.
5. Henry, G. D., and Sykes, D. B. (1994) *Methods Enzymol. 239*, 515−535.
6. Cross, T. A., and Opella, S. J. (1994) *Curr. Opin. Struct. Biol. 4*, 574−581.
7. Opella, S. J., Kim, Y., and McDovell, P. (1994) *Methods Enzymol. 239*, 536−560.
8. Smith, S. O. (1996) *Magn. Reson. Rev. 17*, 1−26.
9. Tycko, R. (1996) *J. Biomol. NMR 8*, 239−251.
10. Tobbet, J. (1987) *Trends Biochem. Sci. 12*, 327−330.
11. Sanders, C. R., Hare, B. J., Howard, K. P., and Prestegard, J. H. (1994) *Prog. NMR Spectrosc. 26*, 421−444.
12. Sanders, C. R., and Landis, G. C. (1995) *Biochemistry 34*, 4030−4040.
13. Sanders, C. R., and Landis, G. C. (1994) *J. Am. Chem. Soc. 116*, 6470−6471.
14. Howard, K. P., and Opella, S. J. (1996) *J. Magn. Reson., Ser. B 112*, 91−94.
15. Boman, A. L., and Kahn, R. A. (1995) *Trends Biochem. Sci. 20*, 147−150.
16. Franco, M., Chardin, P., Chabre, M., and Paris, S. (1996) *J. Biol. Chem. 271*, 1573−1578.
17. Antonny, B., Beraud-Dufour, S., Chardin, P., and Chabre, M. (1997) *Biochemistry 36*, 4675−4684.
18. Amor, J. C., Harrison, D. H., Kahn, R. A., and Ringe, D. (1994) *Nature 372*, 704−708.
19. Sankaram, M. B. (1994) *Biophys. J. 67*, 105−112.
20. Bodanszky, M. (1984) *The practice of peptide synthesis*, Springer-Verlag, New York.
21. Chang, C., Waki, M., Ahmad, M., Meienhofer, J., Lundell, E. O., and Haug, J. D. (1980) *Int. J. Pept. Protein Res. 15*, 59−66.
22. Fields, G. B., and Noble, R. L. (1990) *Int. J. Pept. Protein Res. 35*, 161−214.
23. Prosser, R. S., Hunt, S. A., DiNatale, J. A., and Vold, R. R. (1996) *J. Am. Chem. Soc. 118*, 269−270.
24. Shaka, A. J., and Freeman, R. (1983) *J. Magn. Reson. 51*, 169−173.
25. Hediger, S., Meier, B. M., Kurur, N. D., Bodenhausen, G., and Ernst, R. R. (1994) *Chem. Phys. Lett. 223*, 283−288.
26. Levy, G. C., and Lichter, R. L. (1979) *Nitrogen-15 Nuclear Magnetic Resonance Spectroscopy*, John Wiley & Sons, New York.
27. Andrec, M., and Prestegard, J. H. (1997) *J. Magn. Reson.* (in press).
28. Saupe, A. (1968) *Angew. Chem., Int. Ed. Engl. 7*, 97.
29. Emsly, J. W., and Lindon, J. C. (1975) *NMR Spectroscopy Using Liquid Crystal Solvents*, Pergamon Press, Oxford, U.K.
30. Diehl, P., and Khetrapal, C. L. (1969) *NMR: Basic Principles and Progress*, Springer-Verlag, New York.
31. Oas, T. G., Hartzell, C. J., McMahon, T. J., Drobny, G. P., and Dahlquist, F. W. (1987) *J. Am. Chem. Soc. 109*, 5956−5962.
32. Sanders, C. R., and Prestegard, J. H. (1992) *J. Am. Chem. Soc. 114*, 7096.
33. Press, W. H., Teukolsky, S. A., Vetterling, W. T., and Flannery, B. P. (1992) *Numerical Recipes in C*, Cambridge University Press, Cambridge, U.K.
34. Bugayevskiy, L. M., and Snyder, J. P. (1995) *Map Projections*, Taylor & Francis, London.
35. Greenfield, N., and Fasman, G. D. (1969) *Biochemistry 8*, 4108−4116.
36. McLaughlin, S., and Aderem, A. (1995) *Trends Biochem. Sci. 20*, 272−276.

BI9717791